THE JOURNAL OF PHYSICAL CHEMISTRY Letters

Surfaces, Interfaces, and Catalysis; Physical Properties of Nanomaterials and Materials

Chemically Selective Imaging of Individual Bonds Through Scanning Electron Energy-Loss Spectroscopy: Disulfide Bridges linking Gold Nanoclusters

Karolina Sokolowska, Zhongyue Luan, Eero Hulkko, Christoph Rameshan, Noelia Barrabes, Vartkess Ara Apkarian, and Tanja Lahtinen

J. Phys. Chem. Lett., **Just Accepted Manuscript** • DOI: 10.1021/acs.jpclett.9b03496 • Publication Date (Web): 15 Jan 2020

Chemically Selective Imaging of Individual Bonds Through Scanning Electron Energy-Loss Spectroscopy: Disulfide Bridges linking Gold Nanoclusters

Karolina Sokołowska,† Zhongyue Luan,‡ Eero Hulkko,†,§ Christoph Rameshan,‖ Noelia Barrabés,‖ Vartkess A. Apkarian,⊥ Tanja Lahtinen*†*

†Department of Chemistry, Nanoscience Center, University of Jyväskylä, P.O. Box 35, 40014 Jyväskylä, Finland.

‡Department of Material Science and Engineering, University of California, Irvine, Irvine, CA 92697, USA.

§Department of Electronics and Nanoengineering, Aalto University, P.O. BOX 11000, FI-00076, Finland.

‖Faculty of Technical Chemistry, Institute of Materials Chemistry, Technische Universität Wien, 1060 Vienna, Austria.

⊥Department of Chemistry, University of California, Irvine, Irvine, CA 92697, USA.

AUTHOR INFORMATION

Corresponding Authors

Email: *karolina.x.sokolowska@jyu.fi*; *tanja.m.lahtinen@jyu.fi*

As proof-of-principle of chemically selective, spatially resolved imaging of individual bonds, we carry out electron energy-loss spectroscopy (EELS) in a scanning transmission electron microscope (STEM) on atomically precise, thiolate-coated, gold nanoclusters linked with 5,5′-bis(mercaptomethyl)-2,2′-bipyridine dithiol ligands. The images allow the identification of bridging disulfide bonds (R-S-S-R) between clusters and X-ray photoelectron spectra (XPS) support the finding.

TOC GRAPHICS

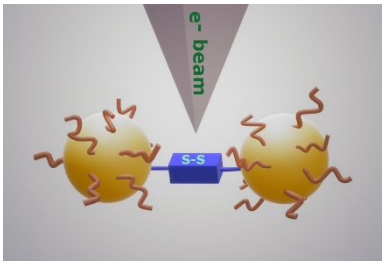

KEYWORDS Gold nanoclusters, linking, Electron energy-loss spectroscopy, X-ray photoelectron spectroscopy.

Rapid progress is being made toward chemically selective atomically resolved microscopy, what may be regarded as the chemists' ideal structural tool. An example is the recent demonstration of imaging vibrational local modes inside a molecule through tip-enhanced Raman spectromicroscopy.[1] This involves measurements in the atomistic near-field, suitable for planar molecules. In contrast, the combination of scanning transmission electron microscopy (STEM) and electron energy-loss (EELS) microscopy provides a far-field method for chemically selective

atom-resolved spectromicroscopy, which has been implemented primarily to image the chemical structure of hard materials.[2-5] Its implementation in soft, organic materials has been limited due to the damage induced by the high energy electrons. With increasing detection sensitivity and energy resolution of electron analyzers, STEM-EELS can be expected to find wider use in direct chemical structure determination, where other methods may fail. We demonstrate this in the present, by imaging the disulfide-bridging bond between atomically precise, thiolate-coated gold nanoclusters, which was anticipated but could not be definitely established by standard spectroscopic means.

Monolayer protected gold nanoclusters have attracted attention due to their physicochemical properties and applications such as surface chemical modification.[6-9] Of interest are gold nanoclusters with >200 gold atoms, which sustain localized surface plasmon resonances (LSPR) that can be tuned by modifying their immediate surroundings.[10,11] Modification of the nanocluster surface is necessary for assembly and implementations in biology, medicine or electronics.[6,7,12] Ligand-exchange reactions are commonly used for this purpose, and bifunctional ligands are used to interconnect nanoclusters into superstructures with tunable optical and electronic properties.[10,12-17] The precisely-defined structural units and their ease in self-assembly allow systematic studies of emergent LSPR properties in individual superstructures, with the recognition that the linkage plays an important role in defining all such properties.[18] A predicate for such studies is the detailed knowledge of the chemical structure.

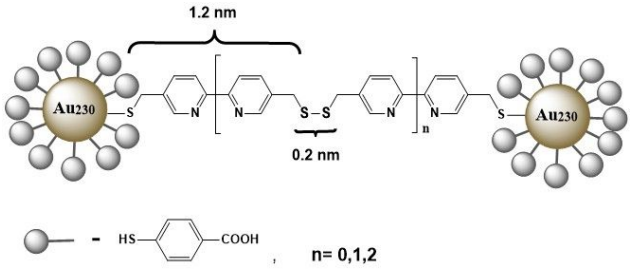

Figure 1. The suggested structure of two Au_{230} nanoclusters linked by 5,5′-bis(mercaptomethyl)-2,2′-bipyridine (BMM-BPy) dithiols. Indicated are the lengths of the dithiol (1.2 nm), and the disulfide bond (0.2 nm).

We recently presented a versatile approach to covalently link $Au_{210\text{-}230}(p\text{-MBA})_{70\text{-}80}$ nanoclusters (Au_{230}) into covalently linked dimers, trimers, and multimers.[17] Based on the analysis of reaction yields and Monte Carlo kinetic models, we speculated on reaction routes involving different linkages:[19] a single dithiol, or two to three dithiols fused by (-S-S-) disulfide bonds, as illustrated in Figure 1. This was indirectly supported by the observation of inter-cluster separations of 1 - 2.85 times the length of a dithiol molecule.[19] However, conclusive spectroscopic proof could not be obtained through methods such as single-particle Raman, because of the spectral congestion by the thiolate-stapled gold clusters. To characterize the individual structures, it is necessary to combine high-resolution microscopy and high-sensitivity spectroscopy.[2,3,20] Electron microscopy has the capability to measure individual nanostructures.[3,4,21,22] STEM has previously been used to characterize the organic/inorganic, thiolate-protected gold nanoclusters on the sub-nanometer scale.[4,22,23] Here, to visualize the linkage, we employ EELS during STEM imaging, as previously implemented to study 2D materials and larger nanoparticles.[3-5] In addition, we exploit X-ray photoelectron spectroscopy (XPS) to provide complementary support.[20] The combination of these analytical tools allows the simultaneous structural and spectral analysis of individual nanostructures.

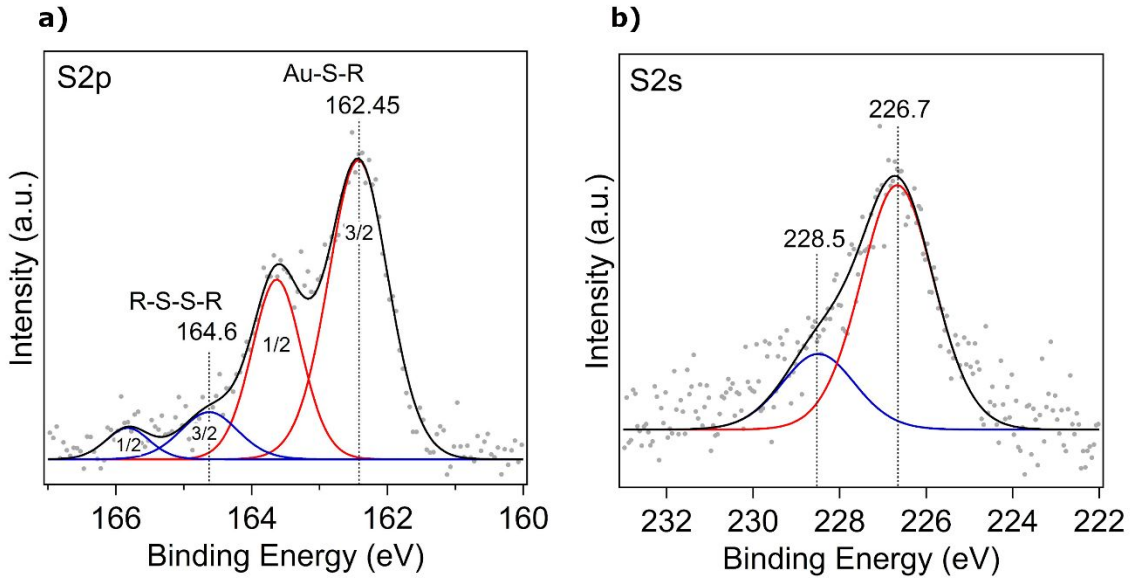

Figure 2. XPS of sulfur (a) 2*p* and (b) 2*s* spectra on Au_{230} linked oligomers. The 2*p* signal is fitted to two spin-orbit split doublets $2p_{1/2}$ and $2p_{3/2}$, and consistent with that, the 2*s* spectrum is fitted to two peaks of the same relative intensity. The red peaks are assigned to S-Au and the blue peaks are assigned to S-S bound sulfur, respectively.

XPS allows elemental analysis of oligomers but lacks the sensitivity to pinpoint individual bonds (See SI experimental methods). The presence of gold, carbon, and a trace amount of oxygen is established through measurements of the core-level spectra of Au 4*f*, C 1*s,* and O 1*s* (Fig. S1). The XPS core-level band around 84 eV is similar to bulk gold, with a linewidth (see Table S1) consistent with nanoclusters of approximately 4 nm in diameter.[20] In Fig. 2, we show the photoemission spectra of the S 2*p* and S 2*s* core-levels. The 2*p* transition consists of spin-orbit split doublets and the spectrum in Fig. 2(a) shows two doublets. The red doublet with the $2p_{3/2}$ component at 162.45 eV is assigned to the sulfur atoms chemically-bonded to gold atoms (S-Au). Similar binding energies at 162.6 eV,[24] 162.8 eV,[25] and 162.9 eV[26] have been observed before in

the thiolate-protected gold nanoclusters. The blue doublet, with $2p_{3/2}$ component at 164.6 eV, is admittedly weak. Confidence in this spectral decomposition is established by its consistency with the S 2*s* spectral profile shown in Fig. 2(b), which is best fitted to two peaks at 226.7 eV and 228.5 eV, with similar relative peak intensities as in the S 2*p* doublet pair. The measured energy of the blue doublet is in excellent agreement with the earlier work of Siegbahn and Verbist, where the same signal at 164.6 eV was assigned to the disulfide group (R-S-S-R) that bridges dithiol molecules.[27] As such, we assign the components at 162.5 eV and 164.6 eV in the S 2*p* band, and 226.7 eV and 228.5 eV in the S 2*s* band to S-Au and S-S bonded sulfur atoms, respectively. The assignment establishes the presence of disulfide bonds but lacks the sensitivity to observe them in individual covalently-linked clusters.

Aberration-corrected STEM images of a monomer, dimer, and trimer of Au_{230} clusters mounted on a graphene-coated grid are shown in Fig. 3(a). The images are obtained at 80 kV, with current and exposure time reduced to minimize e-beam damage, while retaining sufficient imaging contrast. Close-ups of individual Au_{230} clusters are provided in Fig S2, where lattice fringes of

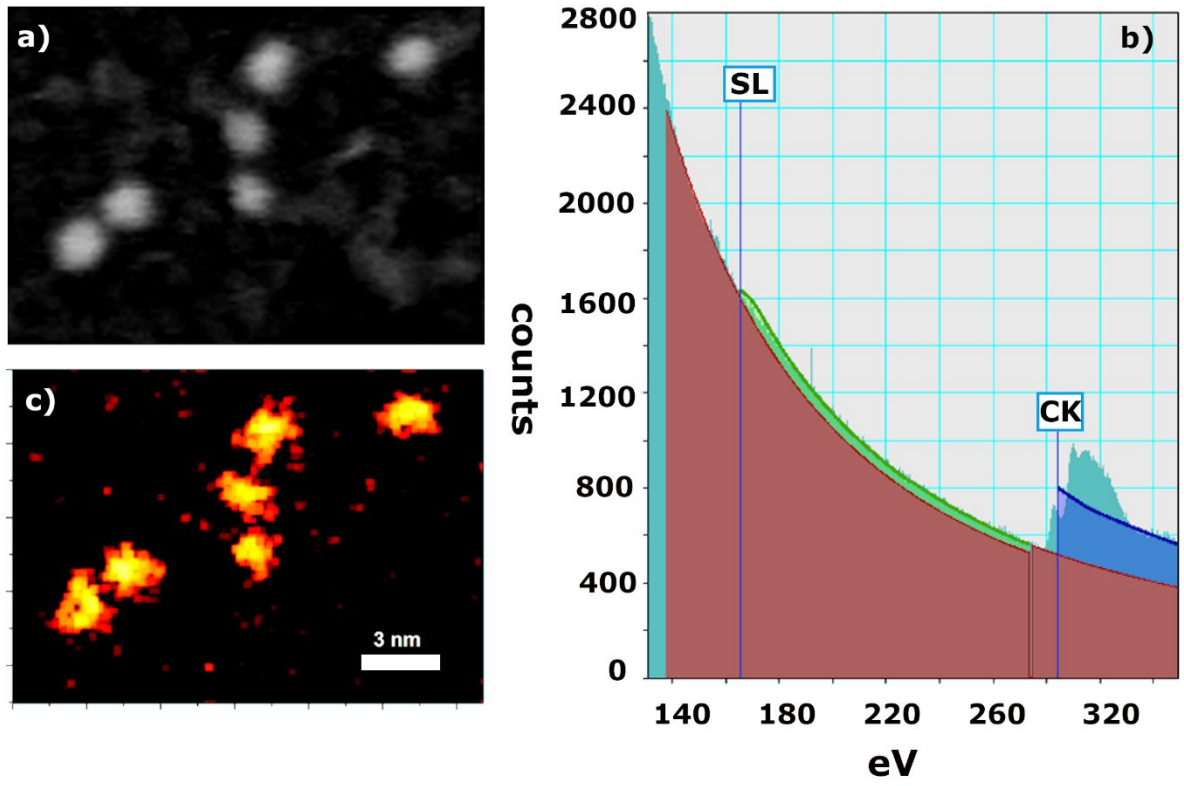

Figure 3. Atomic-level EELS mapping of covalently-linked gold oligomers: (a) STEM image, (b) EELS spectrum showing the opening of scattering channels at S L-edge and C K-edge, (c) Logarithmic intensity plot of the sulfur elemental map.

the face-centered-cubic arrangement can be seen, and the cluster diameter can be established as ~1.8 nm, in agreement with our prior estimate of 1.7±0.1 nm.[28] The sample was prepared by dispersing a trimer solution purified by polyacrylamide gel electrophoresis (PAGE), however an overview of the dry-mounted clusters shows a wide distribution of superstructures (see Fig. S3). As earlier described,[19] dithiol-linked gold structures are dynamic in nature: they undergo continuous breaking and forming of superstructures. The EELS spectrum recorded under the same STEM imaging conditions is shown in Figure 3(b). In the core loss region >100 eV, the spectrum shows the characteristic edges of sulfur (165 eV), carbon (284 eV) dominated by the graphene

grid, and trace amounts of nitrogen (401 eV) and oxygen (532 eV). The complete EELS spectrum is provided in Figure S4. The integrated S loss channel (highlighted in green in Fig. 3b) is mapped in Fig. 3(c) and Figure S5. The maps image the 70-80 sulfur atoms distributed on each $Au_{210-230}$(*p*-MBA)$_{70-80}$ cluster (close-ups provided in Fig. S6).

Line profiles of the elemental sulfur images in Figure 4 explore the inter-cluster bridges. The four images contain the variations seen (for close-ups, see Figs. S6 and S7). In Figs. 4(a) and (b), we see a clear intensity peak between the linked dimers, suggestive of a disulfide bond. Note, the pixel resolution is 0.16 nm, as such the two S atoms of the 0.2 nm-long S–S bond cannot be expected to be resolved. The intensity profile along the orange line in Fig. 4(c) is informative. It shows a peak between the first two clusters, similar to those in 4(a), (b). No such peak is found between the subsequent pairs. Indeed, the inter-cluster separation between clusters 2-3 and 3-4 of ~ 1 nm could only accommodate a single dithiol linker, and therefore a disulfide bond is not expected. The image of an isolated dimer bound by a single 1.2 nm dithiol, absent bridging sulfur, is provided in Fig. S8. In Fig. 4(d), we show the sulfur intensity profiles along with two-line cuts of a trimer. The orange line cuts across two nanoclusters, while the vertical cyan line passes through all three. The profile along the orange line is similar to those in Fig. 4(a) and (b), consistent with a disulfide linkage. The profile along the cyan line shows additional weak peaks ~0.5 nm apart between nanoclusters separated by ~1.5 nm, consistent with two disulfide bridges, therefore three dithiol molecules linking the two nanoclusters. In all cases, the intercluster separations are consistent with the expected number of dithiol linkers, and the visualized disulfide bonds, in full agreement with our prior hypothesis and finding on distances between nanoclusters (1- 2.85 times the length of BMM-BPy.

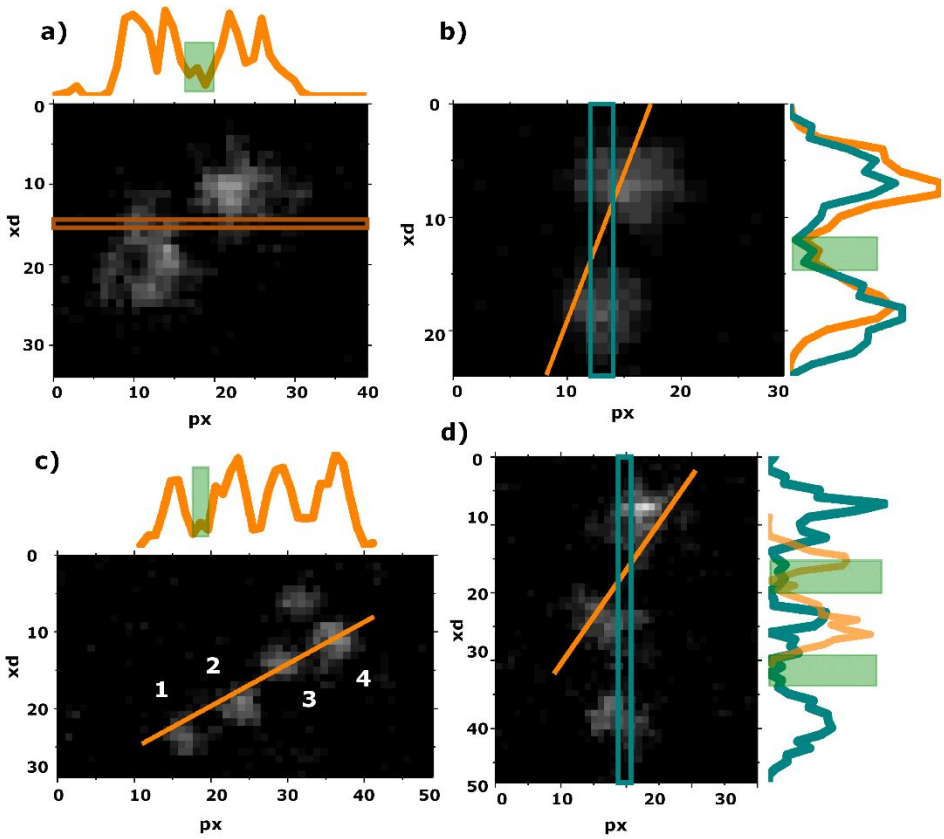

Figure 4. (a)—(d) The cross-section profiles of sulfur intensities taken along the lines indicated in the inset images. The inset images 4(a)—(d) are the same as the enlarged yellow-coded images shown in S5(a)—(d), respectively.

We have demonstrated that the combination of STEM and EELS already allows the visualization of chemical bonds and structure in real space. In the present implementation, we determined the disulfide linkages between dithiol-bound Au_{230} clusters, which to date was the subject of speculation. The nature and composition of the molecular bridges were also confirmed through XPS measurements. The combination of the three techniques provides comprehensive chemical analysis, which can be expected to have broader use as the resolution and sensitivity electron microscopies advance. The particular finding here, namely the bonding motif between

nanoclusters is important to advance our understanding of the optical and electronic response of superstructures with emergent plasmonic response.

ASSOCIATED CONTENT

Supporting Information. The Supporting Information is available free of charge on the ACS Publications website at DOI:

Description of the experimental methods and measurements; Au 4*f*, C 1*s,* and O 1*s* photoemission spectra along with the FWHM values; STEM micrographs of gold nanoclusters; EELS spectrum of covalently-linked nanoclusters; intensity plot of sulfur elemental map derived from EELS spectrum; cross-section profiles of sulfur intensities.

AUTHOR INFORMATION

Corresponding authors

*K.B.S: E-mail: karolina.x.sokolowska@jyu.fi

*T.M.L: E-mail: tanja.m.lahtinen@jyu.fi

ORCID

Eero Hulkko: 0000-0002-7536-5595

Christoph Rameshan: 0000-0002-6340-4147

Noelia Barrabés: 0000-0002-6018-3115

Vartkess Ara Apkarian: 0000-0002-7648-5230

Tanja Lahtinen: 0000-0002-1747-6959

Notes

The authors declare no competing financial interest.

ACKNOWLEDGMENT

This work was supported by the National Science Foundation Center for Chemical Innovation on Chemistry at the Space-Time Limit (CaSTL), grant number CHE-1414466. STEM-EELS characterization was performed at the user facilities of the UC Irvine Materials Research Institute (IMRI), including instrumentation funded in part by the National Science Foundation Major Research Instrumentation Program under grant no. CHE-1338173. We thank Dr. Toshiro Aoki for support to measure STEM-EELS at IMRI and C.R. for providing XPS spectra. We acknowledge Zhipei Sun and Mika Pettersson for fruitful discussions and financial support.

REFERENCES

(1) Lee, J.; Crampton, K. T.; Tallarida, N.; Apkarian A.V. Visualizing Vibrational Normal Modes of a Single Molecule with Atomically Confined Light. *Nature*, **2019**, *568*, 78-82.

(2) Römer, I.; Wang, Z. W.; Merrifield, R. C.; Palmer, R. E.; Lead, J. High-Resolution STEM-EELS Study of Silver Nanoparticles Exposed to Light and Humic Substances. *Environ. Sci. Technol*., **2016**, *50*, 2183–2190.

(3) Arenal, R.; De Matteis, L.; Custardoy, L.; Mayoral, A.; Tence, M.; Grazu, V.; De La Fuente, J. M.; Marquina, C.; Ibarra, M. R. Spatially-Resolved EELS Analysis of Antibody Distribution on Biofunctionalized Magnetic Nanoparticles. *ACS Nano*, **2013**, *7*, 4006–4013.

(4) Bahena, D.; Bhattarai, N.; Santiago, U.; Tlahuice, A.; Ponce, A.; Bach, S. B. H.; Yoon, B.; Whetten, R.L.; Landman, U.; Yacaman, M.J. STEM Electron Diffraction and High-Resolution Images Used in The Determination of the Crystal Structure of The $Au_{144}(SR)_{60}$ Cluster. *J. Phys. Chem. Lett*., **2013**, *4*, 975–981.

(5) Koh, A. L.; Bao, K.; Khan, I.; Smith, W. E.; Kothleitner, G.; Nordlander, P.; Maier, S. A.; McComb, D. W. Electron Energy-Loss Spectroscopy (EELS) of Surface Plasmons in Single Silver Nanoparticles and Dimers: Influence of Beam Damage and Mapping of Dark Modes. *ACS Nano*, **2009**, *3*, 3015–3022.

(6) Calard, F.; Wani, I. H.; Hayat, A.; Jarrosson, T.; Lère-Porte, J.-P.; Jafri, S. H. M.; Serein-Spirau, F.; Leifer, K.; Orthaber, A.; Designing Sterically Demanding Thiolate Coated AuNPs for Electrical Characterization of BPDT in a NP–Molecule–Nanoelectrode Platform. *Mol. Syst. Des. Eng*., **2017**, *2*, 133–139.

(7) Goswami, N.; Zheng, K.; Xie, J.; Bio-NCs – The Marriage of Ultrasmall Metal Nanoclusters with Biomolecules. *Nanoscale*, **2014**, *6*, 13328–13347.

(8) Jin, R.; Zeng, C.; Zhou, M.; Chen, Y.; Atomically Precise Colloidal Metal Nanoclusters and Nanoparticles: Fundamentals and Opportunities. *Chem. Rev*., **2016**, *116*, 10346-10413.

(9) Pezzato, C.; Maiti, S.; Chen, J. L.-Y.; Cazzolaro, A.; Gobbo, C.; Prins, L.J.; Monolayer Protected Gold Nanoparticles with Metal-Ion Binding Sites: Functional Systems for Chemosensing Applications. *Chem. Commun*., **2015**, *51*, 9922-9931.

(10) Halas, N. J.; Lal, S.; Chang, W.-S.; Link, S.; Nordlander, P.; Plasmons in Strongly Coupled Metallic Nanostructures. *Chem. Rev*., **2011**, *111*, 3913–3961.

(11) Li, W.; Physics Models of Plasmonics: Single Nanoparticle, Complex Single Nanoparticle, Nanodimer, and Single Nanoparticle over Metallic Thin Film. *Plasmonics*, **2018**, *13*, 997–1014.

(12) Chakraborty, I.; Pradeep, T.; Atomically Precise Clusters of Noble Metals: Emerging Link between Atoms and Nanoparticles. *Chem. Rev*., **2017**, *117*, 8208-8271.

(13) Azubel, M.; Kornberg, R.D.; Synthesis of Water-Soluble, Thiolate-Protected Gold Nanoparticles Uniform in Size. *Nano Lett*., **2016**, *16*, 3348–3351.

(14) Compel, W. S.; Wong, O. A.; Chen, X.; Yi, C.; Geiss, R.; Häkkinen, H.; Knappenberger, K. L.; Ackerson, C. J.; Dynamic Diglyme-Mediated Self-Assembly of Gold Nanoclusters. *ACS Nano*, **2015**, *9*, 11690- 11698.

(15) Sels, A.; Salassa, G.; Cousin, F.; Lee, L.-T.; Bürgi, T.; Covalently Bonded Multimers of $Au_{25}(SBut)_{18}$ As a Conjugated System. *Nanoscale*, **2018**, *10*, 12754–12762.

(16) Jupally, V. R.; Kota, R.; Van Dornshuld, E.; Mattern, D.L.; Tschumper, G.S.; Jiang, D.-E.; Dass, A.; Interstaple Dithiol Cross-Linking in $Au_{25}(SR)_{18}$ Nanomolecules: A Combined Mass Spectrometric and Computational Study. *J. Am. Chem. Soc*., **2011**, *133*, 20258–20266.

(17) Lahtinen, T.; Hulkko, E.; Sokołowska, K.; Tero, T.-R.; Saarnio, V.; Lindgren, J.; Pettersson, M.; Häkkinen, H.; Lehtovaara, L.; Covalently Linked Multimers of Gold Nanoclusters $Au_{102}(p\text{-MBA})_{44}$ and $Au_{\sim 250}(p\text{-MBA})_{n}$. *Nanoscale*, **2016**, *8*, 18665–18674.

(18) Malola, S.; Lehtovaara, L.; Enkovaara, J.; Häkkinen, H.; Birth of the Localized Surface Plasmon Resonance in Monolayer-Protected Gold Nanoclusters. *ACS Nano*, **2013**, *7*, 10263-10270.

(19) Sokołowska, K.; Hulkko, E.; Lehtovaara, L.; Lahtinen, T.; Dithiol-Induced Oligomerization of Thiol-Protected Gold Nanoclusters. *J. Phys. Chem. C*, **2018**, *122*, 12524–12533.

(20) Zhang, P.; X-ray Spectroscopy of Gold–Thiolate Nanoclusters. *J. Phys. Chem. C*, **2014**, *118*, 25291–25299.

(21) Vergara, S.; Lukes, D. A.; Martynowycz, M. W.; Santiago, U.; Plascencia-Villa, G.; Weiss, S. C.; De La Cruz, M. J.; Black, D. M.; Alvarez, M. M.; López-Lozano, X.; et. al.; MicroED Structure of Au_{146}(*p*-MBA)$_{57}$ at Subatomic Resolution Reveals a Twinned FCC Cluster. *J. Phys. Chem. Lett.*, **2017**, *8*, 5523–5530.

(22) Azubel, M.; Koh, A. L.; Koyasu, K.; Tsukuda, T.; Kornberg, R. D.; Structure Determination of a Water-Soluble 144-Gold Atom Particle at Atomic Resolution by Aberration-Corrected Electron Microscopy. *ACS Nano*, **2017**, *11*, 11866–11871.

(23) Azubel, M.; Koivisto, J.; Malola, S.; Bushnell, D.; Hura, G. L.; Koh, A. L.; Tsunoyama, H.; Tsukuda, T.; Pettersson, M.; Häkkinen, H.; Kornberg, R.D.; Electron Microscopy of Gold Nanoparticles at Atomic Resolution. *Science*, **2014**, *345*, 909–912.

(24) Gobbo, P.; Biesinger, M. C.; Workentin, M. S.; Facile Synthesis of Gold Nanoparticle (AuNP)–Carbon Nanotube (CNT) Hybrids Through an Interfacial Michael Addition Reaction. *Chem. Commun*., **2013**, *49*, 2831–2833.

(25) Gobbo, P.; Mossman, Z.; Nazemi, A.; Niaux, A.; Biesinger, M. C.; Gillies, E. R.; Workentin, M. S.; Versatile Strained Alkyne Modified Water-Soluble AuNPs

for Interfacial Strain Promoted Azide–Alkyne Cycloaddition (I-SPAAC). *J. Mater. Chem. B*, **2014**, *2*, 1764–1769.

(26) Gobbo, P.; Novoa, S.; Biesinger, M. C.; Workentin, M. S.; Interfacial Strain-Promoted Alkyne–Azide Cycloaddition (I-SPAAC) for The Synthesis of Nanomaterial Hybrids. *Chem. Commun.*, **2013**, *49*, 3982–3984.

(27) Lindberg, B. J.; Hamrin, K.; Johansson, G.; Gelius, U.; Fahlman, A.; Nordling, C.; Siegbahn, K.; Molecular Spectroscopy by Means of ESCA II. Sulfur compounds. Correlation of electron binding energy with structure. *Phys. Scr.*, **1970**, *1*, 286–298.

(28) Sokołowska, K.; Malola, S.; Lahtinen, M.; Saarnio, V.; Permi, P.; Koskinen, K.; Jalasvuori, M.; Häkkinen, H.; Lehtovaara, L.; Lahtinen, T.; Towards Controlled Synthesis of Water-Soluble Gold Nanoclusters: Synthesis and Analysis. *J. Phys. Chem. C*, **2019**, *123*, 2602–2612.